Chapter 1 Introduction

In the recent years, wireless communication has attracted a lot of attention. It brings enormous information with a great convenience at low cost. And a number of researches to the wireless network have risen beyond all expectation. There are many wireless communication standards in the world, among which the IEEE 802.11 (a/ b/ g/ n) are most widely used. The operated frequency band in 802.11a is from 5.14GHz to 5.875GHz. But 802.11b, 802.11g, and 802.11n standards use the 2.4 GHz band. Because of this choice of frequency band, 802.11b and 802.11g equipment will suffer interference from microwave ovens, cordless telephones, Bluetooth devices, baby and security monitors, amateur radio and other appliances using this same band. In the contrast, 802.11a devices are not affected by products operating on the 2.4 GHz band. These standards use spectrum resources which are not licensed to result in multi-limitation. Therefore, many solutions are actively proposed and still under development. A new group of smart antenna designs is one of these possible solutions. Antenna design is an important role in the WLAN system as is well known to all. A good antenna may help improve the performance of WLAN no matter in the field of data rate, transmitting distance, and so on. Smart antenna (also known as adaptive antenna) refers to a system of antenna arrays with smart signal processing algorithms that are used to identify the direction of arrival signal, and use it to calculate beam-forming vectors, to track and locate the antenna beam on the mobile target. Smart antenna techniques are used notably in acoustic signal processing, track and scan RADAR, radio astronomy and radio telescopes, and mostly in cellular systems like W-CDMA and UMTS. Moreover, smart antennas have two main functions: direction of arrival estimation and Beam-forming technique.

Beam-forming technique can be broadly divided into two categories: conventional switched beam antennas and adaptive array antennas. Conventional switched beam antennas use a fixed set of weightings and phasings to combine the signals from the sensors in the array, primarily using only information about the location of the sensors in space and the wave directions of interest. In contrast, adaptive array antenna, generally combine this information with properties of the signals actually received by the array, typically to improve rejection of unwanted signals from other directions. That is, an adaptive beamformer is able to adapt automatically its response to different situations. Obviously, adaptive array antennas are the better consideration for the future development of WLAN.

An ideal smart beam-forming antenna prototype therefore arises. Antenna which is without any extra equipments and modulation process making the direction of arrival under control easily is a desirable property. Moreover, a compact structure, broadband technique, and multiple functionalities have also become considerable design criteria.

For utilizing a limited spectrum efficiently, the technology of radiation reconfigurable antennas [1]-[10] is used to be applied often. It is an excellent candidate to reduce the multi-path interference and power consumption because of adaptive pattern and high gain. Among these antenna configurations, there are several investigations of adaptive antennas which are based on Yagi-Uda antenna design [4]-[10]. These conventional antennas consist of a radiating dipole in the center with plenty of parasitic elements in the arbitrary circumstance. In [4], the conventional dipoles have been replaced by monopoles. Whereas in [5]-[7], the antennas maintain the basic Yagi-Uda antenna but the parasitic monopole elements around the active monopole antennas are loaded alternatively, either short or open. Because the load attached to the parasitic monopoles alters the effective length of monopoles, the

electromagnetic interactions between monopoles result in pattern beam-forming. Some of the parasites are settled in the shape of circle [5]-[7]; some of them are in the shape of radioactive rays [7]. As for parasitic elements, cylindrical rod monopoles are used in [5], [7], and cylindrical rod monopoles with disc plates which help reducing the height of antenna are disclosed in [6]. However, it needs a plenty of rod monopoles to reach pattern beam-forming and high gain.

In this paper, we propose a new configuration of improved reconfigurable antenna which provides more flexible design of pattern beam-forming. And the printed strip monopoles [8]-[10] on the substrate are often considered for use instead of the three-dimensional rod monopole, which reduces the complexity substantially. The printed parasitic monopoles are length-tunable with the method of directly changing the length of short-ended parasitic monopoles by switches [10]. In this work, the parasitic elements are all shorted unlike the conventional parasites with alternatively loaded. There are three antenna examples proposed in this work. The first example consists of three elements; two length-tunable parasitic monopoles by switches located oppositely to an active strip element. Three elements are perpendicular to the rectangular ground plane. According to the Yagi-Uda antenna, when the length of the parasitic element is shorter than that of the active element, it has a pulling pattern. Oppositely, if the length of the parasitic element is longer than that of the active element, it has a pushing pattern. The directivity of radiation pattern is hence under control. As for the second example, there are five elements totally: two length-tunable parasitic elements located each side of the active element. The effects of increasing the number of the parasitic elements are revealed as expectation. The pattern is more concentrated, and the HPBW is narrower. Furthermore, to augment the performance of pattern beam-forming the number of the length-tunable parasitic element has been expanded to eight in the last example, that is, there are nine elements in total. The

nine parasitic elements are set to the shape of a crisscross. It can be inferred easily that the different combination of switch states result in multiple directivities. As a result, there are four kinds of directivities, four cases, obtained in the simulation. These four cases can be switched arbitrarily by the additional control circuit in different application depending on the operation situation and location of access point.

Chapter 2 Theory of Yagi-Uda antenna and monopole

2.1 Yagi-Uda antenna

From the description in [15], we know that array antennas can be used to increase directivity. Array feed networks are considerably simplified if only a few elements are fed directly. Such an array is referred to as a parasitic array. The elements that are not directly driven (called parasites) receive their excitation by near field coupling from the active element. A famous parasitic array of parallel dipoles is called Yagi-Uda antenna. In this section, the theory of Yagi-Uda antenna is disclosed in detail because the proposed antenna in this thesis is modified from it.

The basic unit of a Yagi-Uda antenna consists of three elements. To understand the principles of operation for a three element Yagi-Uda antenna, we must begin with a driven element and add parasites to it. Consider a driven element that is a resonant half-wave dipole. If a parasitic element is positioned very close to it, we say 0.04λ, it is excited by the driven element with roughly equal amplitude, so the field incident on the parasite is

$$E_{incident} = E_{driver} \tag{2-1}$$

A current is excited on the parasite and the resulting radiated electric field, also tangent to the wire, is equal in amplitude and opposite in phase to the incident wave. This is because the electric field arriving at the parasite from the driver is tangential to it and the total electric field tangential to a good conductor is zero. Thus, the field radiated by the parasite is such that the total tangential field on the parasite is zero, which gives

$$E_{parasite} = -E_{incident} = -E_{driver} \tag{2-2}$$

Therefore, the pattern of this simple two-element array is shown as

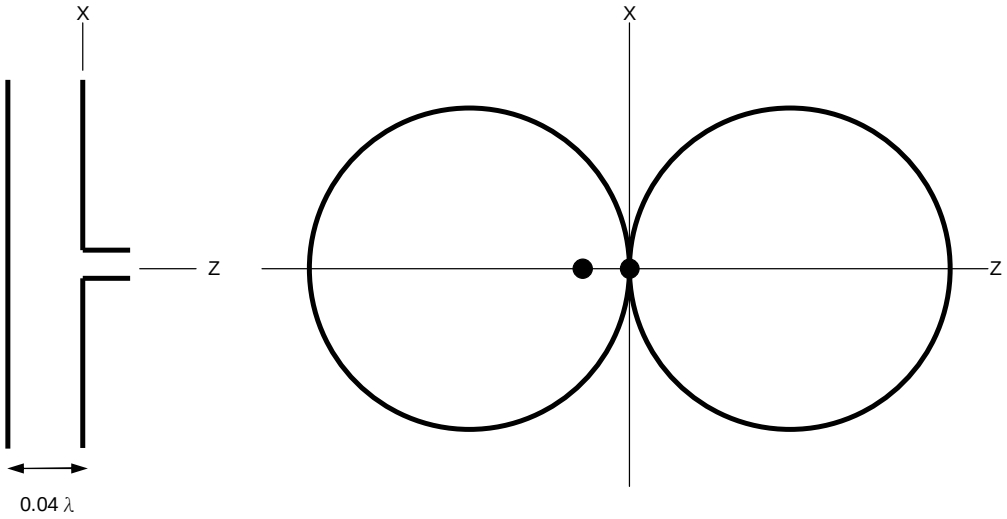

(a) Array configuration (b) H-plane pattern

Fig. 2.1.1 A two-element array of half-wave resonant dipoles, one a driver and the other a parasite. The currents on both are equal in amplitude and opposite in phase.

The simplistic beauty of the Yagi-Uda is revealed by lengthening the parasitic. The dual endfire beam is changed to a more desirable single endfire beam. This effect is illustrated in Fig.2.1.2 for the two-element array. The driver is a dipole of length 0.4781λ, which is a half-wave resonant length when operated in free space. The parasite is a straight wire of length 0.49λ away from the driver. As a result, a single main beam occurs in the endfire direction from the parasite to the driver along the line of array. Such a parasite is called a reflector because it appears to reflect radiation from the driver. If the parasite is shorter than the driver, but placed on the other side of the driver, the pattern elects is similar to that when using a reflector in the sense that main beam enhancement is in the same direction. The parasite is then referred to as a director since it appears to direct radiation in the direction from the driver toward the director. The parasitic array in Fig.2.1.3(a) consisting of a driver and a director has the pattern shown in Fig.2.1.3(b)

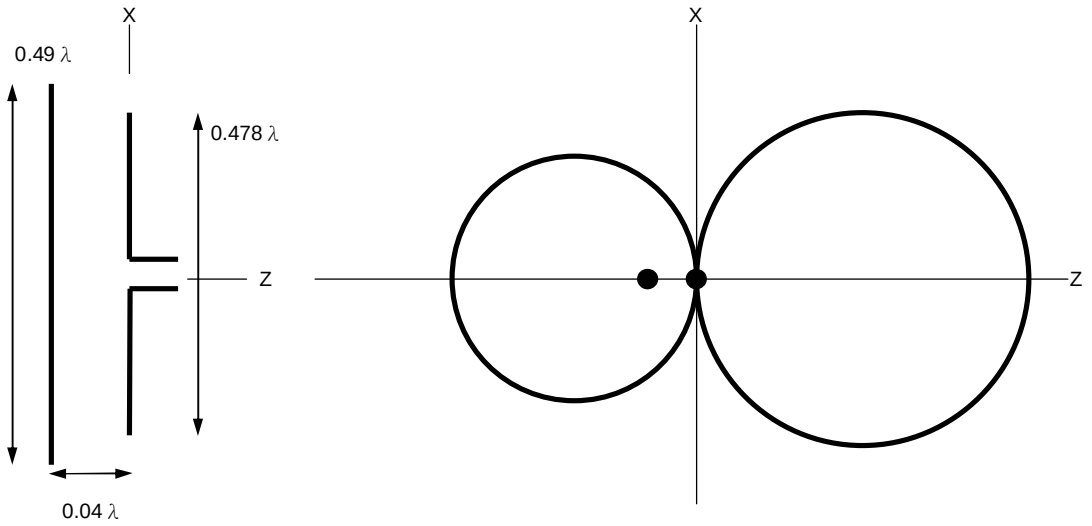

(a) Array configuration (b) H-plane pattern

Fig. 2.1.2 A half-wave dipole with a reflector.

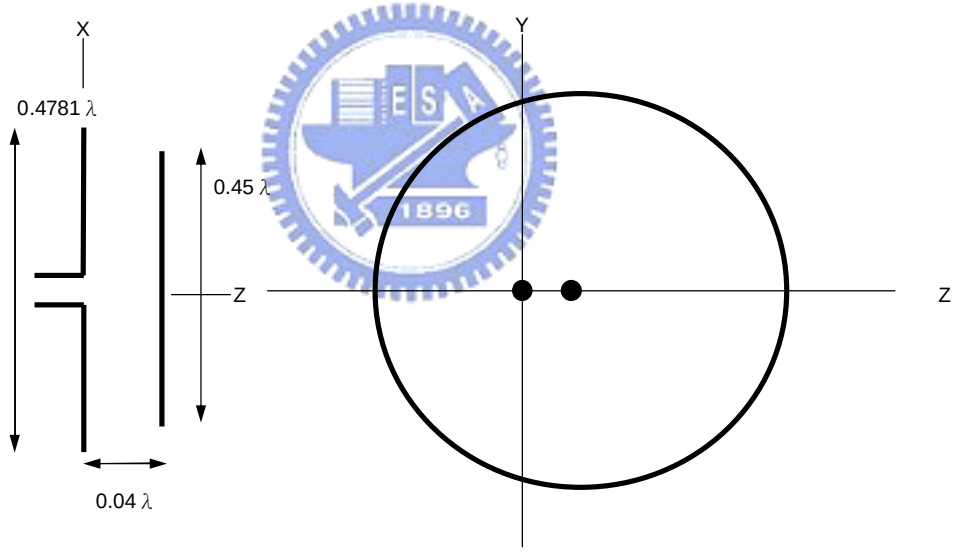

(a) Array configuration (b) H-plane pattern

Fig. 2.1.3 A half-wave dipole with a director.

The single endfire beam created by the use of a reflector or a director alone with a driver suggests that even further enhancement could be achieved with a reflector or a director on opposite sides of driver. This is indeed the case. An example of a three-element Yagi-Uda is shown in Fig.2.1.4(a), which is a combination of the

geometries of Fig.2.1.2(a) and Fig.2.1.3(a). The pattern of Fig.2.1.4(b) is improved over that of either two-element array.

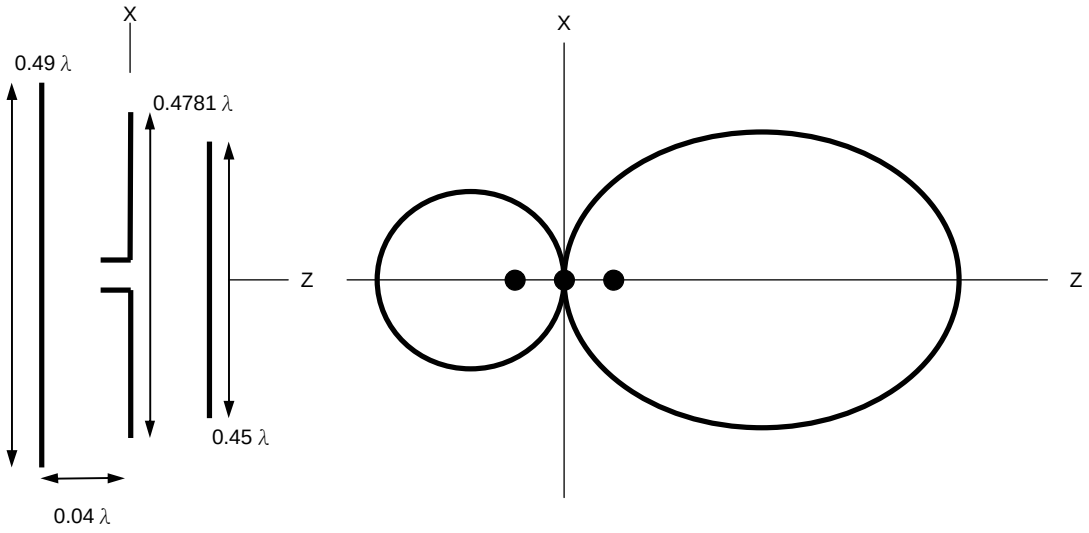

(a) Array configuration (b) H-plane pattern

Fig. 2.1.4 Three-element Yagi-Uda antenna consisting a driver dipole, a reflector, and a director. The wire radius is all 0.001 λ

2.2 Monopole antenna

From the previous paragraph, half-wave wire dipole structure is used in Yagi-Uda antenna. Half-wave dipole is a very common structure actually. The current whose amplitude varies as one-half of a sine wave with a maximum at the center is linear distributed. The three-dimensional pattern of half-wave dipole is like a donut. The pattern on H-plane is omni-direction, which explains the half-wave dipole is widely used in WLAN application. The current distribution is written as

$$I(z) = I_m \sin\left[\beta\left(\frac{\lambda}{4} - |z|\right)\right], \qquad |z| \le \frac{\lambda}{4} \tag{2-3}$$

I_m ：maximum value of current

β：phase constant in free space

From this current, we can find the electric field and magnetic field as

$$E_\theta = j\eta \frac{I_0 e^{-jkr}}{2\pi r}\left[\frac{\cos\left[\left(\pi/2\right)\cos\theta\right]}{\sin\theta}\right] \tag{2-4}$$

$$H_\phi = j\frac{I_0 e^{-jkr}}{2\pi r}\left[\frac{\cos\left[\left(\pi/2\right)\cos\theta\right]}{\sin\theta}\right] \tag{2-5}$$

And the power pattern is defined as

$$P(\theta) = \frac{U(r,\theta)}{U_{\max}} = \left[\frac{\cos(\frac{\pi}{2}\cos\theta)}{\sin\theta}\right]^2 \tag{2-6}$$

Therefore, the current distribution and radiation pattern of a half-wave dipole are shown as follows

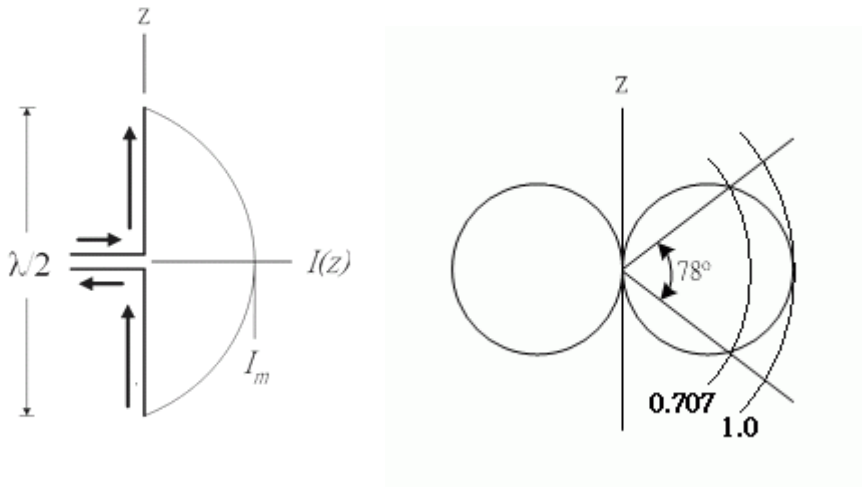

(a) Array configuration (b) pattern and half power beamwidth

Fig. 2.2.1 A common half-wave dipole antenna

One very important description of an antenna is how much it concentrates energy in one direction in preference to radiate in other directions. This characteristic of an antenna is called directivity. And the directivity is defined as

$$D = \frac{P(\theta)_{\max}}{P_{av}} \tag{2-7}$$

In we consider the real world case. When the operated frequency happens to be the resonated frequency of antenna, the power in transmission feeding to the antenna is distortion absolutely for the natural loss of material. That is, the radiation efficiency can be defined as

$$\varsigma = \frac{P_{RAD}}{P_{RAD} + P_{ohm}} \tag{2-8}$$

The relation between the power gain, radiation efficiency, and directivity is than be found as

$$G = \varsigma D \tag{2-9}$$

As for monopole antenna is merely a simplified modification from dipole antenna. By using the image theorem with the help of a extent ground plane, a quarter-wave monopole is easily inferred. The structure of quarter-wave monopole and its current distribution on it are clearly disclosed in Fig.2.2.2.

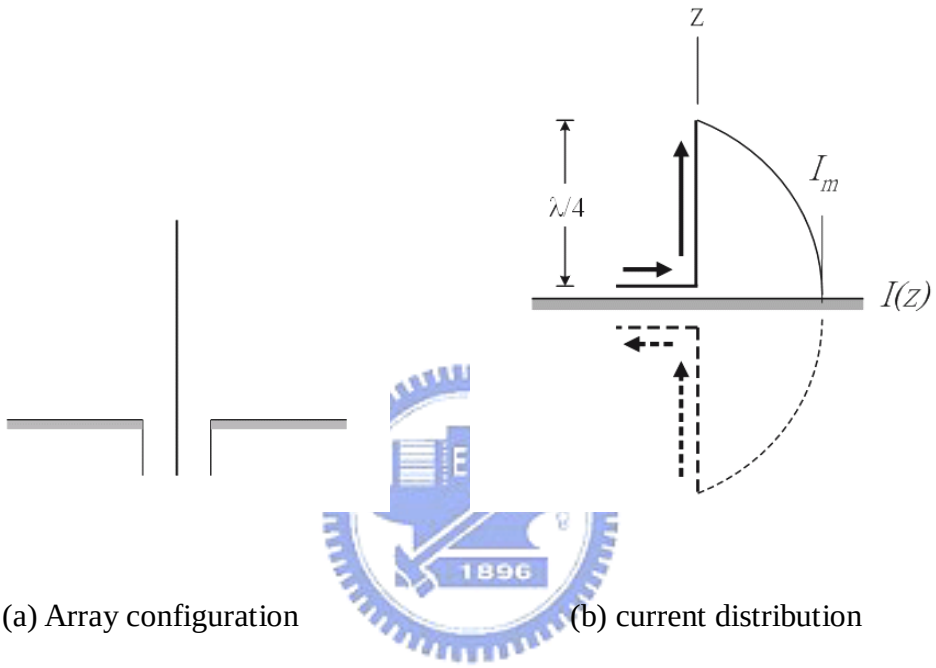

(a) Array configuration (b) current distribution

Fig. 2.2.2 quarter-wave monopole antenna

Since the current distribution on the upper side of monopole and dipole are the same, and the practical length is reduced from one-half to one-fourth wavelength, the input impedance of monopole is calculated as

$$Z_{A,monopole} = \frac{V_{A,monopole}}{I_{A,monopole}} = \frac{\frac{1}{2}V_{A,dipole}}{I_{A,dipole}} = \frac{1}{2}Z_{A,dipole} \tag{2-10}$$

Because the maximum unit area radiate power of dipole and monopole are equal, the length of dipole is double to that of monopole. The directivity of monopole is twice of

that of dipole eventually.

$$D_{monopole} = 2D_{dipole} \tag{2-11}$$

Chapter 3 Pattern reconfigurable antenna

3.1 Pattern reconfigurable antenna configuration

According to the Yagi-Uda antenna, the pattern beam-forming is mainly controlled by the directors and reflectors which are determined by the effective length of the parasitic element. In this thesis, a novel pattern reconfigurable antenna is proposed, which is fabricated of microstrip technology due to low profile, light weight, and easy modification. The half-wave dipole is replaced by quarter-wave monopole, and the wire is replaced by printed circuit on PCB. All printed elements are strips on the FR4 microwave substrate with the thickness of 0.8mm and the dielectric constant of 4.4. The active monopole is 2.4mm wide for 50ohms feeding at operated frequency, 2.45GHz, and the parasitic elements are set to be 1.5mm wide. We use the switch positioned on the parasites to change the effective length that decides parasites function as a director or a reflector directly [10]. When the switch is off, the parasitic element is cut into two pieces: a short ended strip at the lower part and an open strip at the upper part that both work as directors. By contrast, when the switch is on, the length of the parasitic element is longer than that of the active element; the printed parasitic element is performed as a reflector. And the influence of different positions of the switches is one of the investigations in this work.

For proof of concepts, a 1.5 mm $\times$ 1.5 mm slot is taken as switch off, and a metal strip is taken as switch on in this work. But practical implementation of switches can make use of MEMs [11], PIN diodes, or even photoconducting switches [12]. Although varactor is another candidate, the applied voltage is relatively high [13] and difficult to implement [14].

3.2 Three-element array

To design a pattern reconfigurable antenna, we must begin with a driven element and add parasites to it. The active element is designed to match the RF port of 50 ohms and resonate at 2.45 GHz, the input impedance is inevitably affected by the appearance of the parasitic elements. Therefore, the horizontal open stub, with the size of 7 mm × 4 mm, is added at the bottom of the active element with a gap of 0.1mm to the ground plane for getting a fine matching.

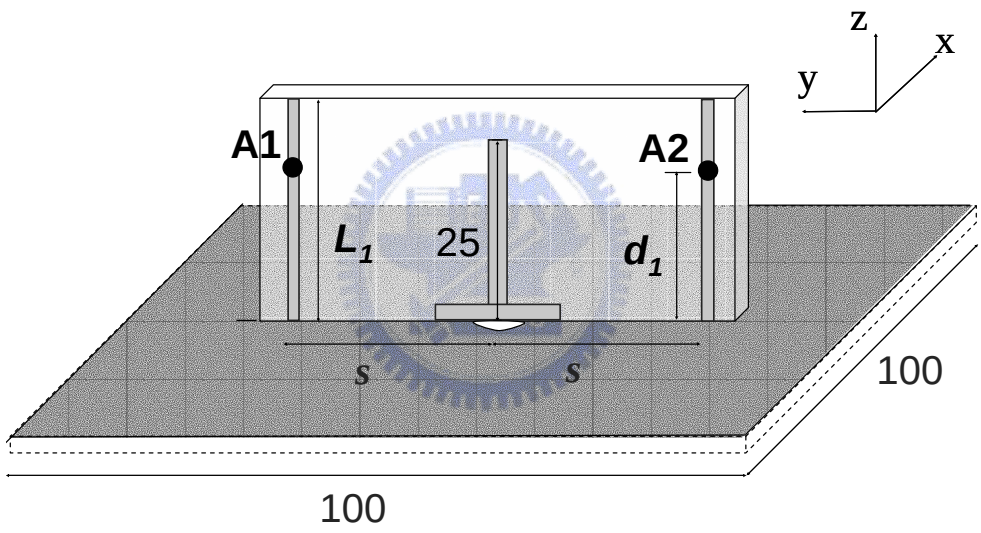

Fig. 3.2.1 three-element array configuration

Then a three-element array antenna example is taken as a preliminary. There are only two printed parasitic elements. Fig. 3.2.1 shows the structure of the three-element array. The active element is placed in the center of the ground, and two printed parasitic elements placed symmetrically are connected to the ground directly. Because of the parasitic elements, the length of the active element (L_a) is 25mm, which is less than the conventional $\lambda_o/4$. The length of the parasitic elements (L_1) is 30mm which is equal to $0.245\lambda_o$. The spacing between elements is *s*. The black spots

show that switches are set on positions A1 and A2 which are under control of parameter d_1, which is the distance from the ground plane to the switch. The size of ground plane is $G_L \times G_w$ = 100mm × 100mm. Fig.3.2.2 shows the return loss responses of three-element array with and without the impedance-matching horizontal stub. By using this horizontal open stub, the return loss is cover the required band and has a deep at 2.5GHz for d_1 = 20 mm.

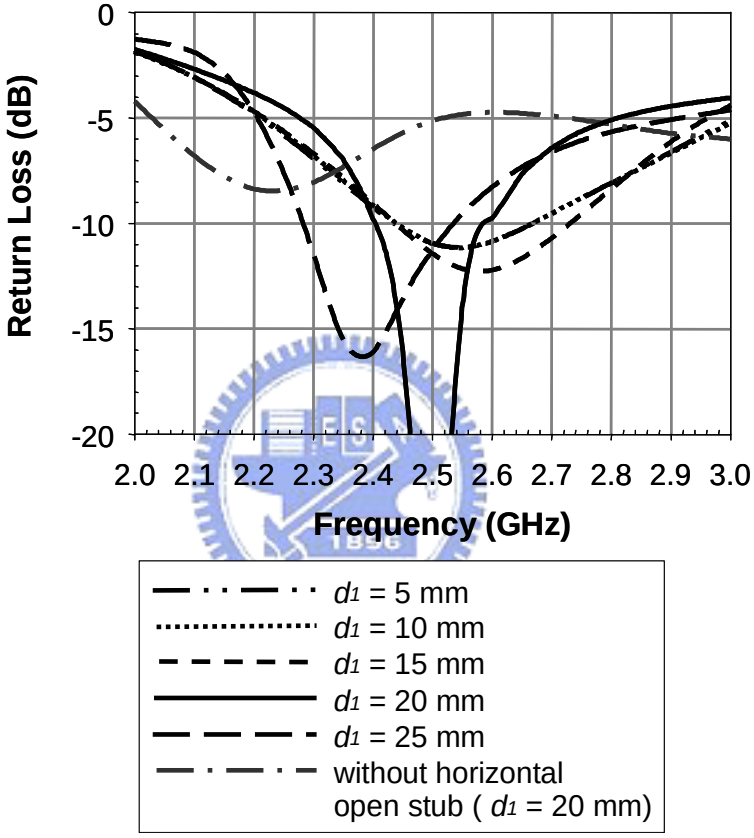

Fig. 3.2.2. The simulated return loss of three-element array when $L_1 = s$ = 30mm. The plot lines of d_1=5mm and d_1=10mm are too close to identify.)

Because the three-element array is the simplest configuration, it is easy to tell if the director and reflector work well. For research convenience, the parasitic element on the +y axis is set to be a reflector (A1 on), whereas the parasitic element on the -y axis is a director (A2 off). We use HFSS, an Ansoft software, to simulate antenna's

performance. From Fig. 3.2.2, the simulated return loss of the three-element array with s = 30 mm, L_1 = 30 mm, and d_1 as a parameter, it can be observed evidently that parasitic elements affect input matching and even improve the operating bandwidth. The bandwidth of d_1 = 20 mm for reflection coefficient below -10dB is from 2.4 to 2.6 GHz.

The pattern performance at 2.45GHz is illustrated in Fig. 3.2.3. The shape of pattern tends towards -y axis as expectation. The maximal gains of different values of d_1 are occurred around the position of $\theta = 310^\circ$, and $\phi = 270^\circ$. From Fig. 3(a), it can be seen the pattern is tilted about 30 degrees from the ground plane. There is a null on the z axis which is an essential characteristic of the active monopole. If we compare the result with the original antenna without any parasitic elements, the maximum gain increases to 5.84 dBi from 3.34 dBi when d_1 is 20 mm. When d_1 = 25 mm the two parasitic elements act like not directors, nor reflectors with no benefit. Hence the directors and reflectors have maximum function when d_1 = 20 mm.

Next parameters going to be discussed are s and L_1, that is, the spacing between monopoles and the length of the parasitic monopoles. Fig. 4 shows the return loss of the three monopoles array with d_1 = 20 mm, L_1 = 30 mm and different values of s. When s is less than 30 mm the input impedance is no longer matched through the whole band (2.4 to 2.5GHz), and the best matching occurs when s = 30 mm. From the simulated patterns by HFSS, when s = 30 mm, the pattern on both yz and xy plane has maximum SLL(side lobe level, unit: mm) and peak gain. Since the length of parasitic monopole should exceed the length of the active monopole when parasitic monopole operates as a reflector, $L_1 \geqq$ 25mm is required. According to the simulation, L_1 has little influence on return loss and pattern beam-forming than s. The optimal value of L_1 for the best return loss response is found to be 30 mm by HFSS. From the above analysis, it is seen that the optimal values of s and L_1 are both 30mm.

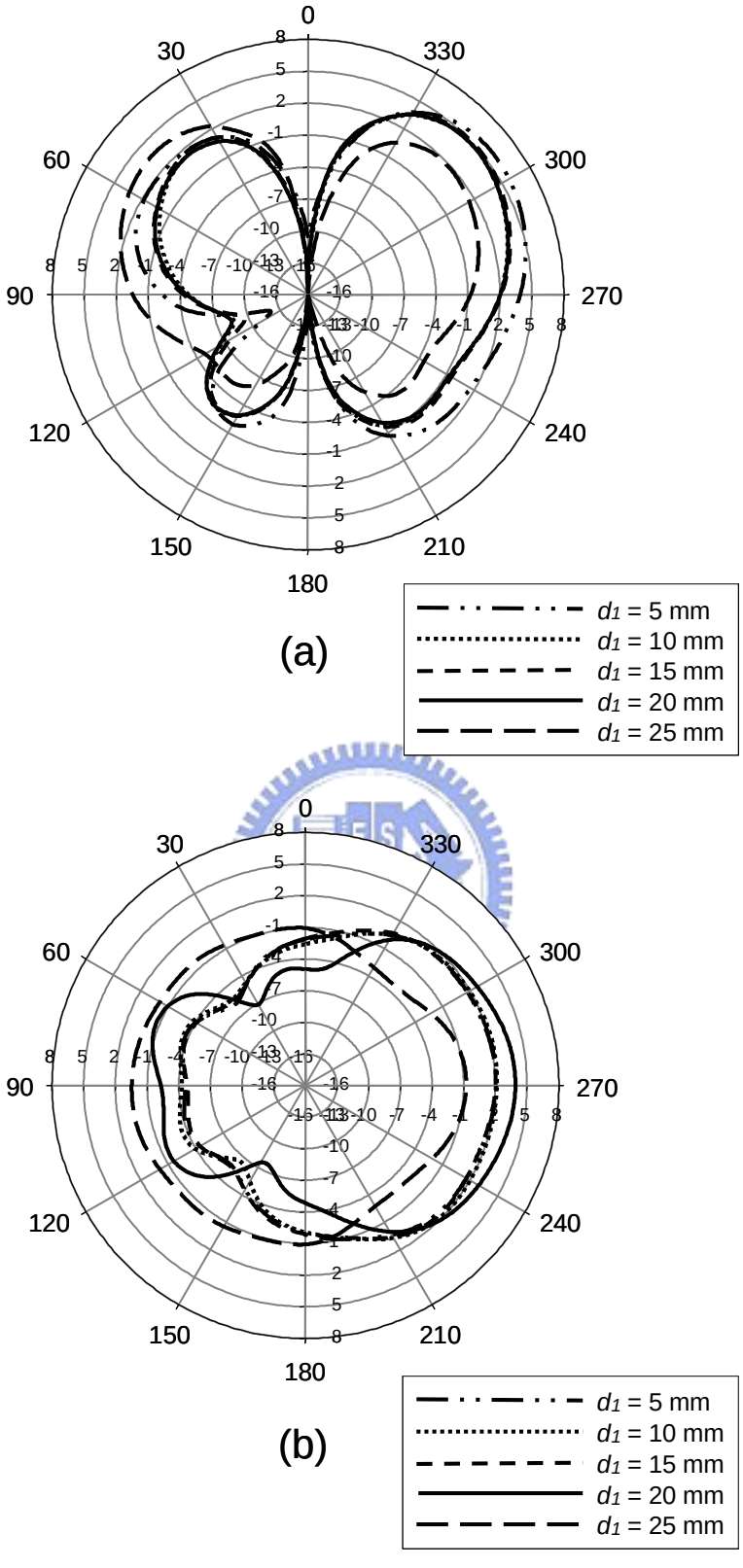

Fig. 3.2.3. The simulated radiation patterns of three-element array for the two primary planes (a) yz plane, and (b) xy plane.

TABLE I

THREE-ELEMENT ARRAY WITH DIFFERENT VALUES OF d_1

	Peak Gain (dBi)	SLL on yz plane	HPBW on yz plane
d_1 = 5	4.87	4.61	70°
d_1 = 10	4.88	3.54	70°
d_1 = 15	5.08	3.44	70°
d_1 = 20	5.84	3.97	80°
d_1 = 25	3.35	1.51	60°

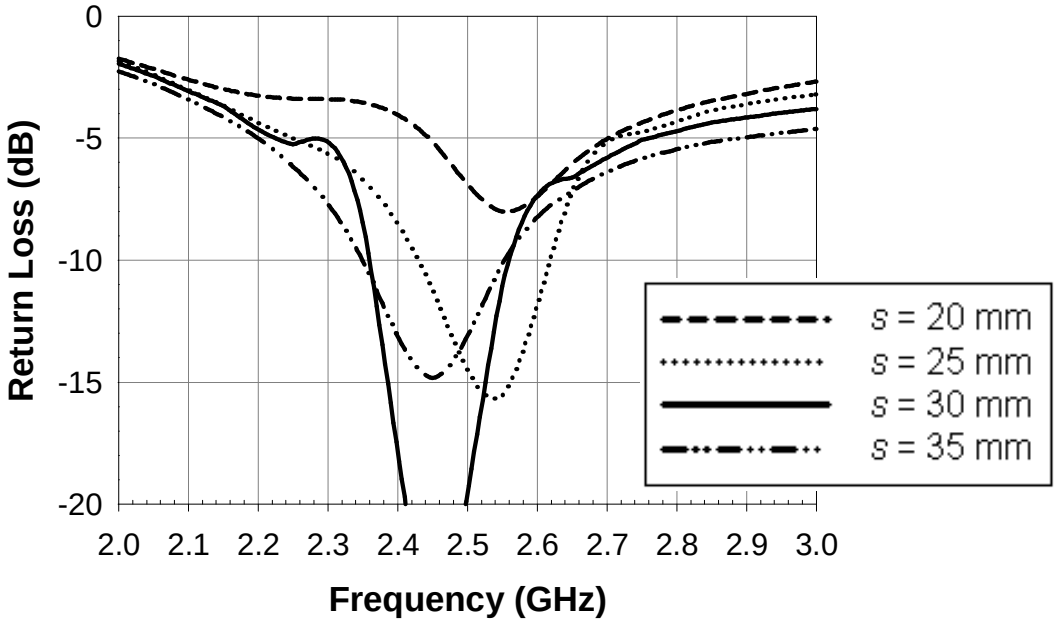

Fig. 3.2.4. The simulated return loss of the three-element array with different values of s, when d_1 = 20 mm, L_1 = 30 mm.

3.3 Five-element array

The second example is five-element array shown in Fig. 3.3.1. The difference is the number of printed parasitic elements around the active elements; as a result of the presence of the extra elements, L_a is varied from 25mm to 24.5mm for better return loss. The second printed parasitic elements (B1 and B2 on them) is added parallel to the first printed parasitic elements (A1 and A2 on them) and separated by *s* as before. The length of the second printed parasitic element is L_2. All of the elements are on the yz plane. The ground plane is therefore enlarged to $G_L \times G_w$ = 140 mm × 140 mm. The switches (B1 and B2) are both at the same position with a distance from the ground plane and controlled by parameter d_2.

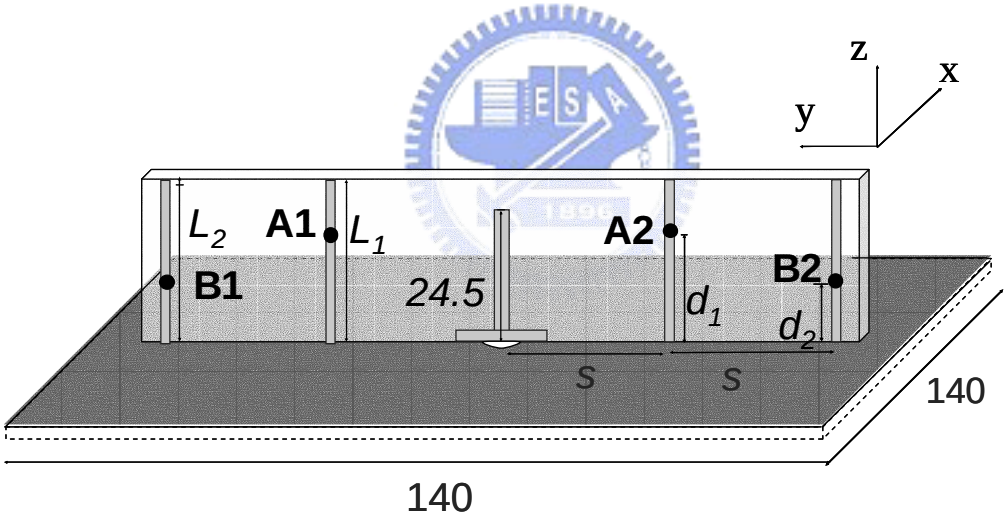

Fig. 3.3.1 Five-element array configuration

Since we know that the parasitic elements affect the performance, the number of the parasitic elements is thus an influential variable as well. The number of parasitic elements rises to two on each side in the five-element array. At the same time, the positions of switches are controlled by d_1 (switches: A1 and A2) and d_2 (switches: B1 and B2) individually. From the previous analysis, the influence of *s* (spacing between

elements) and L (length of parasitic element) is less than the dominate parameter d_1, so the second parasitic element is added in the same dimension with the first parasitic elements and separated in the same spacing with each other at the preliminary design. After the optimization by HFSS, the length and spacing of the second parasitic elements (with switches: B1 and B2) is identical to the first parasitic elements (with switches: A1 and A2), that is, $L_1 = L_2 = 30$ mm. These parasitic elements on the +y axis are set to be reflectors (A1 and B1 on). In this circumstance, Fig. 3.3.2 shows how the different values of d_1 and d_2 affect the peak gains. From Fig. 3.3.2, it is obvious that d_1 is the dominant parameter deciding the peak gain. The comparatively larger peak gain occurred around $d_1 / L_1 = 0.66$, that is, $d_1 = 20$ mm. And the local maximum peak gain is occurred when $d_2 / L_2 = 0.16$, 0.31, 0.5, and 0.92.

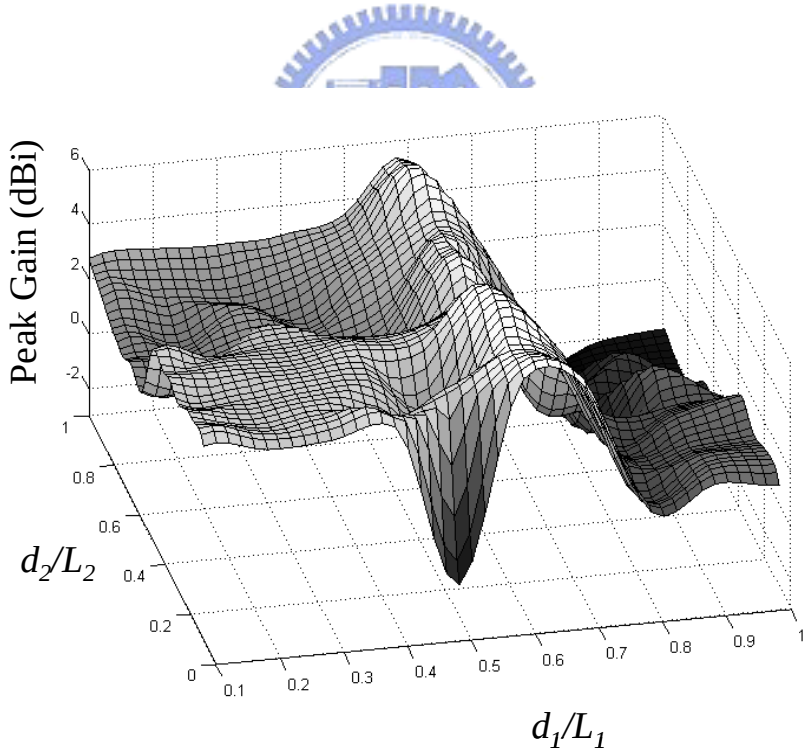

Fig. 3.3.2. The simulated values of peak gain for different values of d_1 / L_1, and d_2 / L_2 when $L_1 = L_2 = 30$ mm.

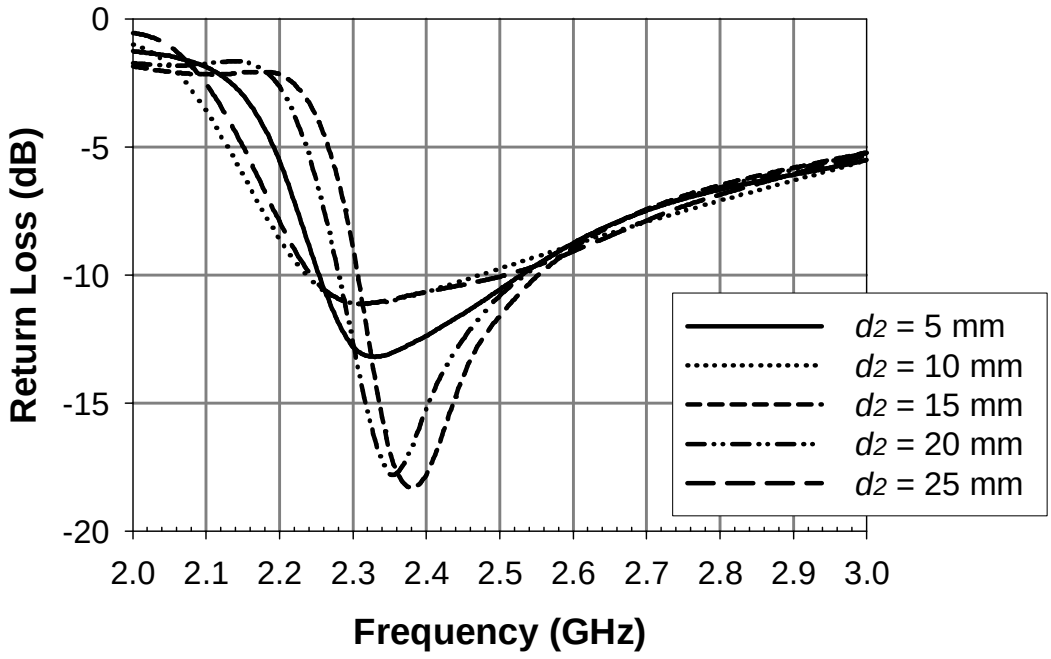

Fig. 3.3.3 The simulated return loss of the five-element array of d_1 = 20 mm and different values of d_2.

Fig. 3.3.3 illustrates the frequency response of the return loss for various values of d_2. Comparing this figure with Fig. 3.1.2, it can be inferred that the return loss is less sensitive to d_2. When d_2= 10 or 25 mm, the responses are too flat. The widest bandwidth is from 2.25 to 2.55 GHz for d_2 = 5 mm, where the required band (2.4 GHz to 2.5 GHz) is covered totally. Fig. 3.3.4 is the simulated radiation patterns of the five-element with various values of d_2. Table Ⅱ displays the peak gain, SLL of the yz cut plane, and HPBW of the yz cut plane. When d_2 = 20 or 25 mm, the bidirectional directivity do not satisfy requirement for their poor peak gain and SLL. As for considering the HPBW, those of d_2 = 15 or 25 mm are relatively wider. As a result of regarding the return loss, peak gain, SLL of the yz plane, and HPBW of the yz plane as the design criteria in this investigation, the most satisfying value of d_2 is 5mm.

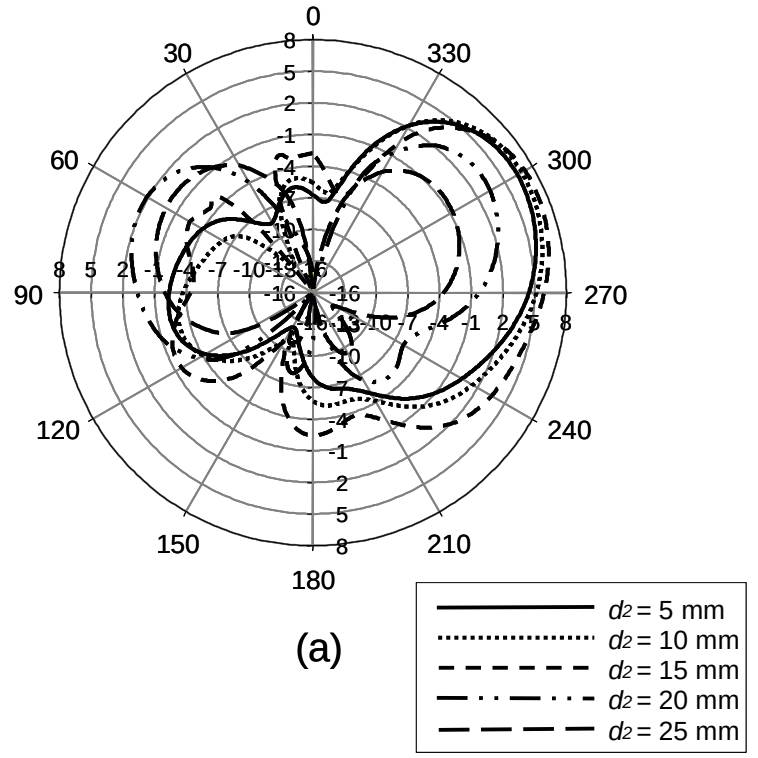

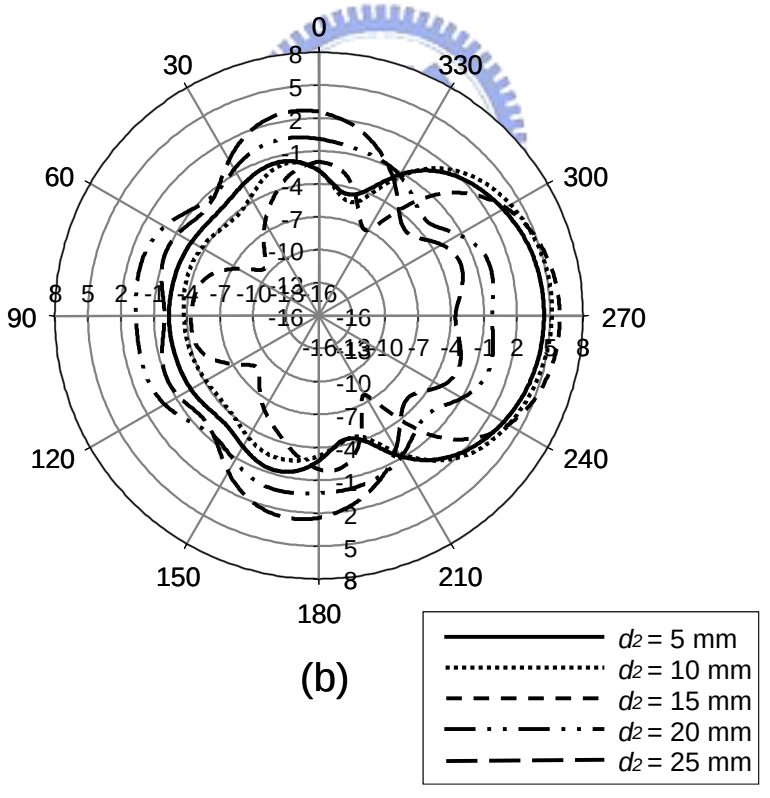

Fig. 3.3.4 The simulated radiation patterns of the five-element array for the two primary planes with d_1 = 20 mm. (a) yz plane, and (b) xy plane.

TABLE Ⅱ

FIVE-ELEMENT ARRAY WITH d_1 = 20 mm AND DIFFERENT VALUES OF d_2

	Peak Gain (dBi)	SLL on yz plane (dBi)	HPBW on yz plane
d_2 = 5	6.37	8.63	50°
d_2 = 10	6.85	9.91	60°
d_2 = 15	7.19	8.87	75°
d_2 = 20	3.38	1.24	50°
d_2 = 25	0.07	0.68	75°

It is worthy to mention that although the second parasitic element has positive effects on the beam-forming, a third parallel parasitic element would be helpless because the current coupling between the active element and the third one is too weak to function.

3.4 Nine-element array

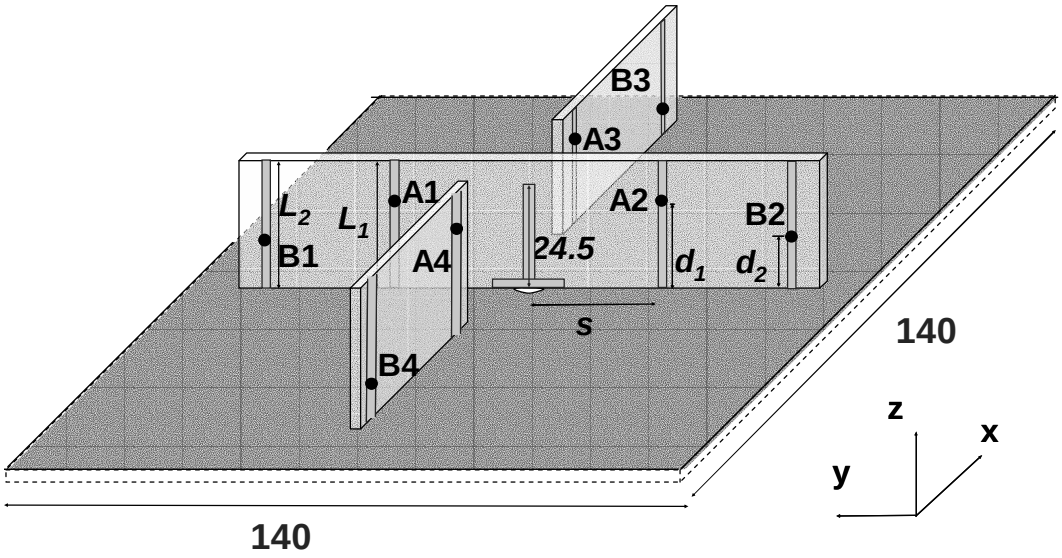

Fig. 3.4.1 Nine-element array configuration

The structure of nine-element array, Fig. 3.4.1, is modified from Fig. 3.3.1 and is the main antenna discussed in this paper. There are nine printed elements shaped as a crisscross, which has the active element at the center still. The dimension of the ground plane is maintained as $G_L \times G_w$ = 140 mm × 140 mm and the dimension of elements are as before. Four switches (A1-A4) of the first printed parasitic elements near the center are adjustable by d_1, and the rest switches (B1-B4) of elements are under control of d_2.

TABLE Ⅲ

SIMPLIFIED NOTATION OF SWITCHABLE PARASITE FUNCTION

Notation	Switch state	Parasite function
0	off	Director
1	on	Reflector

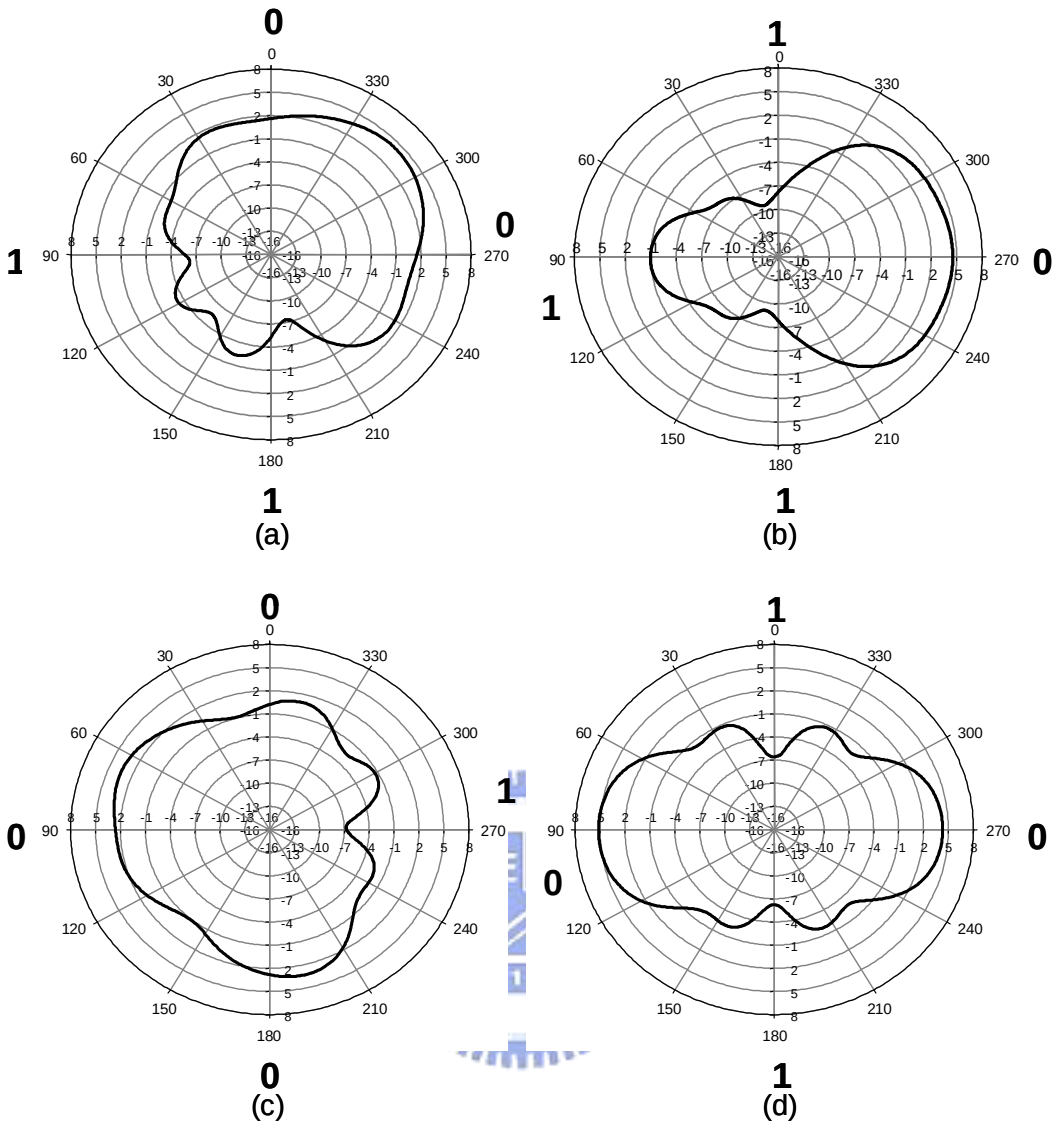

Fig. 3.4.2 The simulated radiation patterns of nine-element array for the four cases shown in Table Ⅳ on the xy plane. (a) case 1 (b) case 2 (c) case 3 (d) case 4 (The boldface number outside the polar plot is the notation of the states of the switches on that direction, that is, 0 for switches off and 1 for switches on).

From the previous simulated results, the most appropriate value of (d_1, d_2) is (20 mm, 5 mm). Now consider the nine crisscross elements array, which is constructed by copying the parasitic elements of five-element array and pasting by a rotation angle of 90 degrees. Thus there are more options of patterns to choose. Since the construction is symmetric, the four directive patterns of the xy plane are shown in Fig. 3.4.2. The

boldface number outside the polar plots is the notation representing the state of switch in that direction. Table Ⅲ explains the rules of notation.

Table Ⅳ displays the detail information of the four cases with different switch states of the nine-element crisscross array. Obviously, the pattern tends towards the direction where the switch states are turned off (represented by number: 0). A maximum peak gain of the nine-element array occurs in case 1, where a peak gain of 6.37 dBi is achieved at the position of $\theta = 300^{\circ}$ and $\phi = 315^{\circ}$. In case 2 and case 3, the patterns are directive, though the HPBWs are very wide. The pattern in case 4 is bidirectional.

As observed from Fig. 3.4.2 and Table Ⅳ, the main beam can be switched to four possible directions ensuring 360 degrees coverage in the H plane in all directive cases. Taking case 1 for example, under setting switches (AB1, AB2, AB3, AB4) = (1, 0, 0, 1), the directivity has main beam on $\phi = 315^{\circ}$. But if we set switches (AB1, AB2, AB3, AB4) = (0, 1, 0, 1), the directivity will have main beam on $\phi = 45^{\circ}$ as anticipation. That is, by different setting of switches state, the main beam could be on $\phi = 45^{\circ}$, 135°, 225°, and 315°. Similarly, the case 2 can provide the main beam on $\phi = 0^{\circ}$, 90°, 180°, and 270°. Therefore, the main beam of nine-element array can then be switched every 45 degrees to cover the whole H plane by using case 1 and case 2. Consequently the nine-element array provides multiple directivities.

Another issue discussed here is the number of the switches used. In the nine-element array configuration, the complexity of implementation is greatly increased due to eight switches if the bias lines are considered. Another practicable solution is to replace switches (B1-B4) of the second parasitic elements by open slots or metal strips. However, the peak gain definitely decreases in these two conditions. So we must trade off between peak gain and circuit complexity.

TABLE Ⅳ.

THE CASES OF THE NINE-ELEMENT ARRAY WITH DIFFERENT SWITCH STATES: “0” FOR SWITCH OFF, WHEREAS “1” FOR SWITCH ON.

Directive cases	case 1	case 2	case 3	case 4
Switches A1, B1	1	1	0	0
Switches A2, B2	0	0	1	0
Switches A3, B3	0	1	0	1
Switches A4, B4	1	1	0	1
Peak gain(dBi)	6.59	6.04	5.68	5.37
Peak gain position	θ=60°, ϕ=315°	θ =70 °, ϕ=270°	θ=60°, ϕ=75°	θ=90°, ϕ=90°
HPBW of xy plane	70°	105°	135°	60°

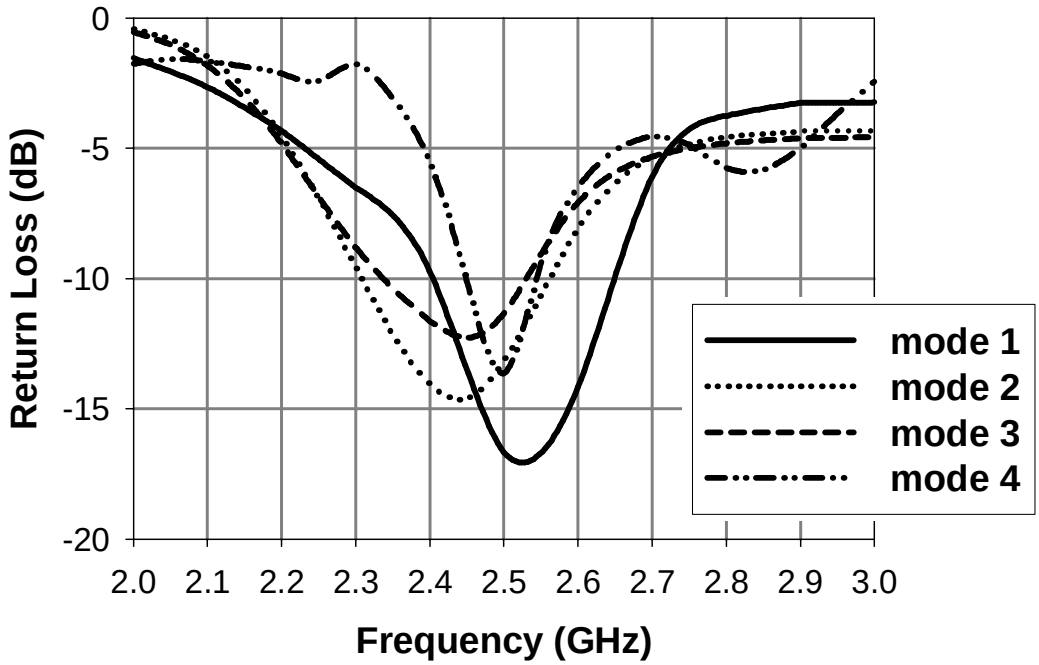

Fig. 3.4.3. The simulated return loss of the nine-element array with four different cases.

Fig. 3.4.3 illustrates the simulated return loss of these four cases. The impedance has a good matching through case 1 to case 3 in the required 2.4 GHz - 2.5 GHz band, with bandwidths larger than 200MHz. By comparison, the bandwidth of case 4 is narrower than the others and is from 2.45GHz to 2.54GHz. Among these four directive cases, case 1 has the widest bandwidth and the maximum peak gain of 6.37dBi. But when all eight switches are turned on or off simultaneously, the pattern has no directivity and the input impedance of antenna is not matched well at the resonance frequency.

Chapter 4 Experimental results

As a result of the previous section, an experimental investigation is undertaken. The three, five, and nine-element array are fabricated respectively. The experimental results are displayed respectively, too.

4.1 Three-element array

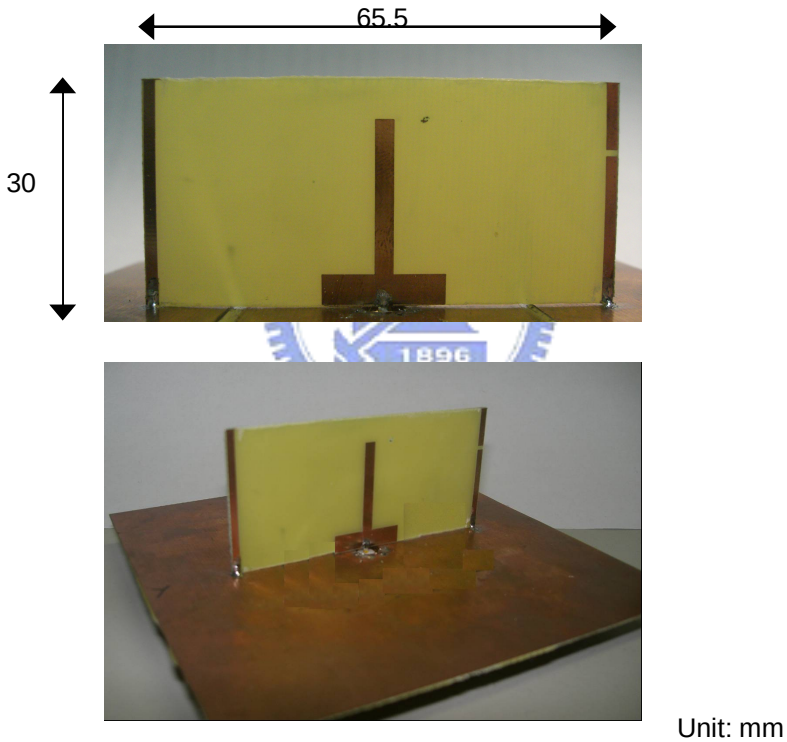

Fig. 4.1.1. Pictures of three-element array.

The prototype of three-element array antenna is established and shown in Fig. 4.1.1. The measured return loss and pattern comparing with simulated data of the three-element array are presented in Fig. 4.1.2 and Fig. 4.1.3. The bandwidth for reflection coefficient below -10dB is from 2.3 to 2.65 GHz in Fig. 4.1.2. Comparing

with the simulated return loss, the bandwidth is increased by 150 MHz, and the return loss at the resonance frequency is not so deep as well though.

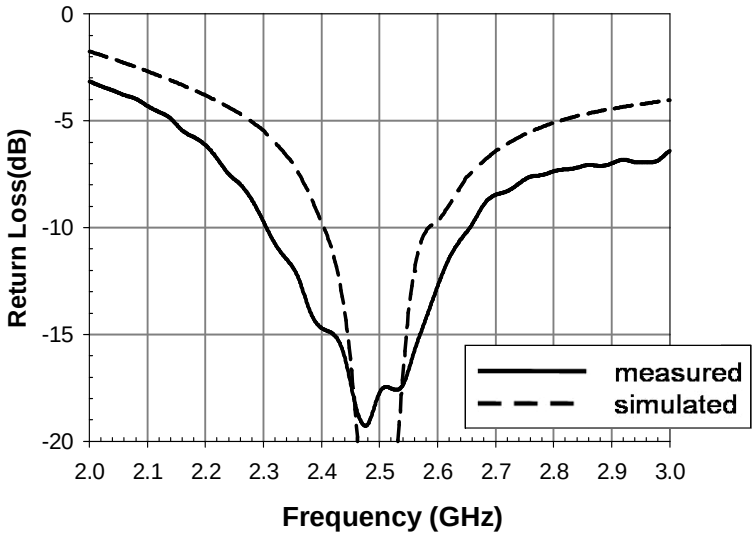

Fig. 4.1.2. Return loss of three-element array.

In Fig. 4.1.3, the pattern from the three-element array shows the measured pattern which has less SLL and narrower HPBW on yz plane. The measured peak gain shown in Fig. 4.1.3. is 5.41 dBi at $\theta = 300^{\circ}$ and $\phi = 27\tilde{0}^{\circ}$. On yz plane, the SLL, front-to-back ratio (FBR), and HPBW are 10.71 dB, 13.24 dB, and 65°, respectively. If the setting of switches A1 and A2 are changed, that is, A1 is off while A2 is on, it is easy to infer that the main beam is toward +y axis inversely. The correlation of these two directivities is rather small.

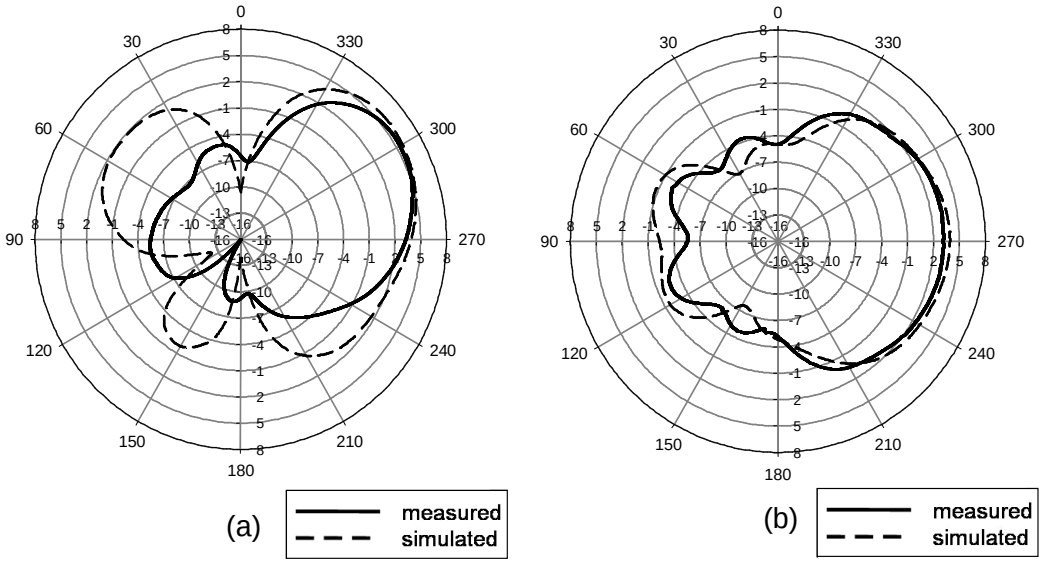

Fig. 4.1.3. The measured pattern of the three-element array at its center frequency, 2.45GHz. (a) yz plane (b) xy plane

4.2 Five-element array

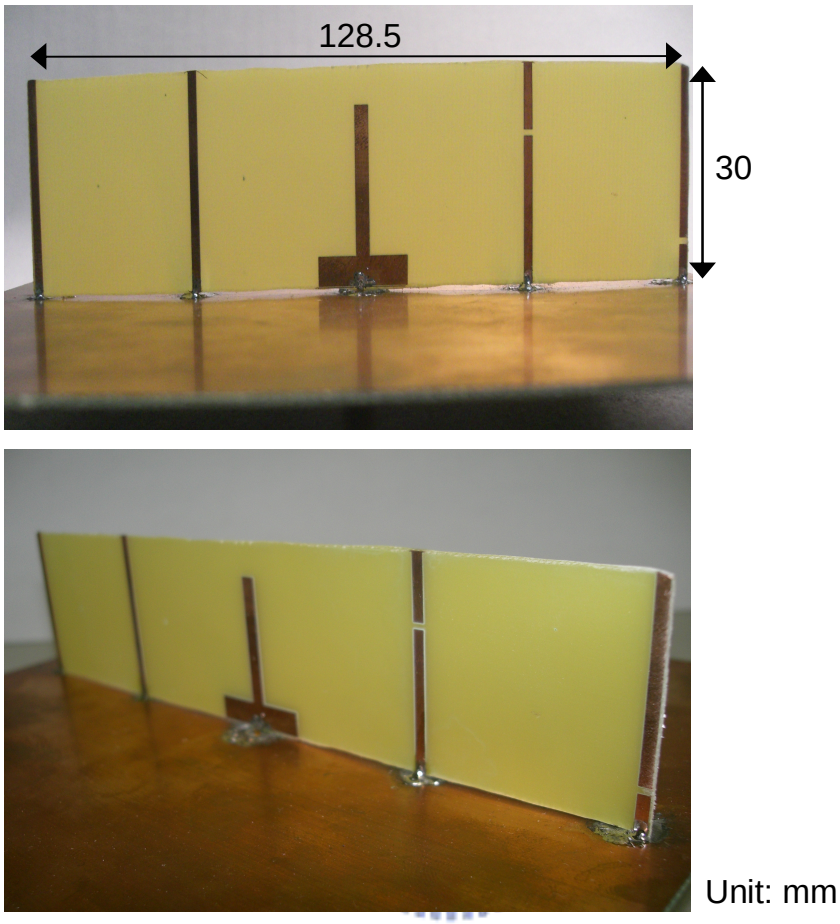

Fig. 4.2.1. Pictures of five-element array.

The prototype of five-element array antenna is established and shown in Fig. 4.2.1. In Fig. 4.2.2, the measured return loss of the five-element array is displayed with the simulated data. Although there is a frequency shift in the simulated return loss, the measured bandwidth for reflection coefficient below -10 dB is from 2.31 to 2.64 GHz, which is very similar to that of the three-element array. It can be inferred that the second parasitic elements (with switches B1-B4) have little influence on the input impedance matching but do help the radiation pattern to achieve higher peak gain. In Fig. 4.2.3, it is evident that the second parasitic elements cause the pattern more tilted

from the ground plane, and the peak gain also increased. The peak gain occurs at θ = 315°, ϕ = 270° with value of 6.95 dBi. In other words, the second parasitic elements improve the peak gain by 1.54 dB. The SLL, FBR, and HPBW of yz plane are 11.01 dB, 12.7 dB, and 63°, respectively.

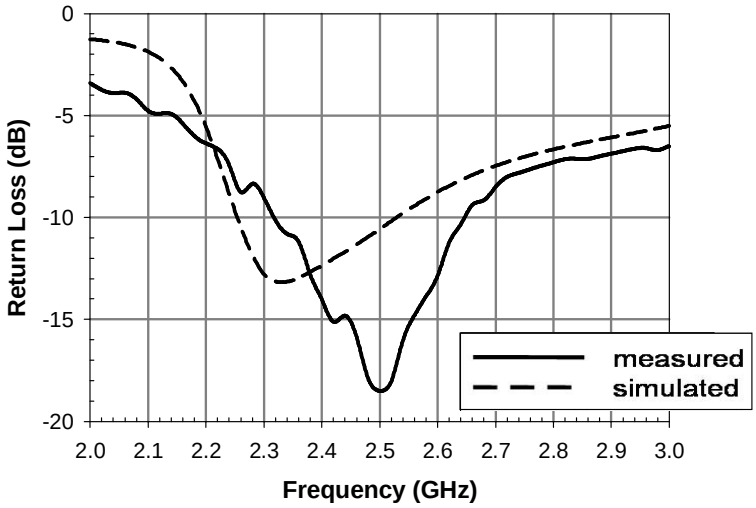

Fig. 4.2.2. The measured return loss of the five-element array.

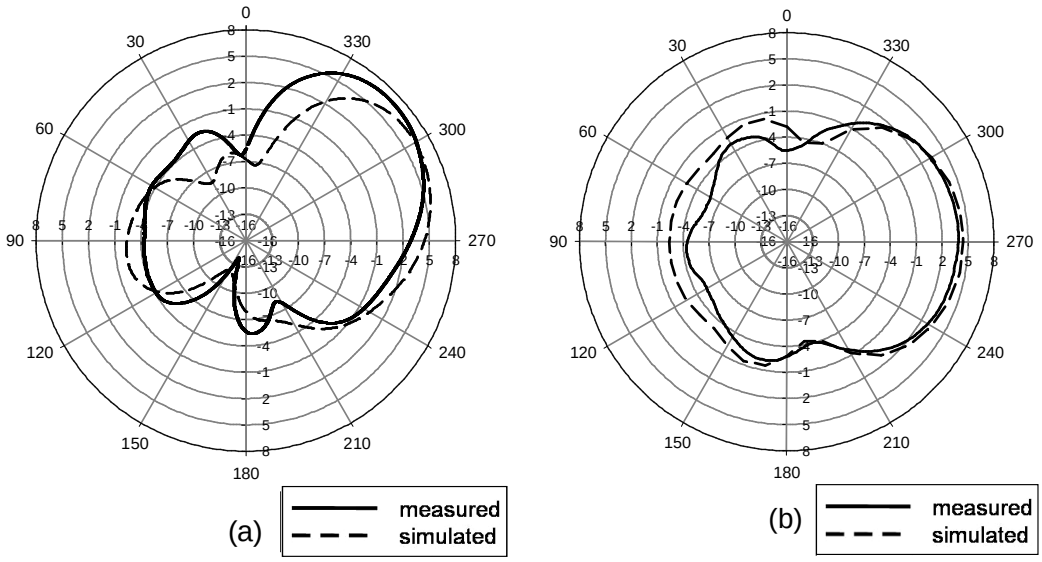

Fig. 4.2.3. The measured patterns of the five-element array at its center frequency, 2.5GHz. (a) yz plane (b) xy plane.

4.3 Nine-element array

From previous sections, a nine-element array is implemented with ideal switch as shown in Fig. 4.3.1. The detail of measured and simulated data comparison is in following paragraphs.

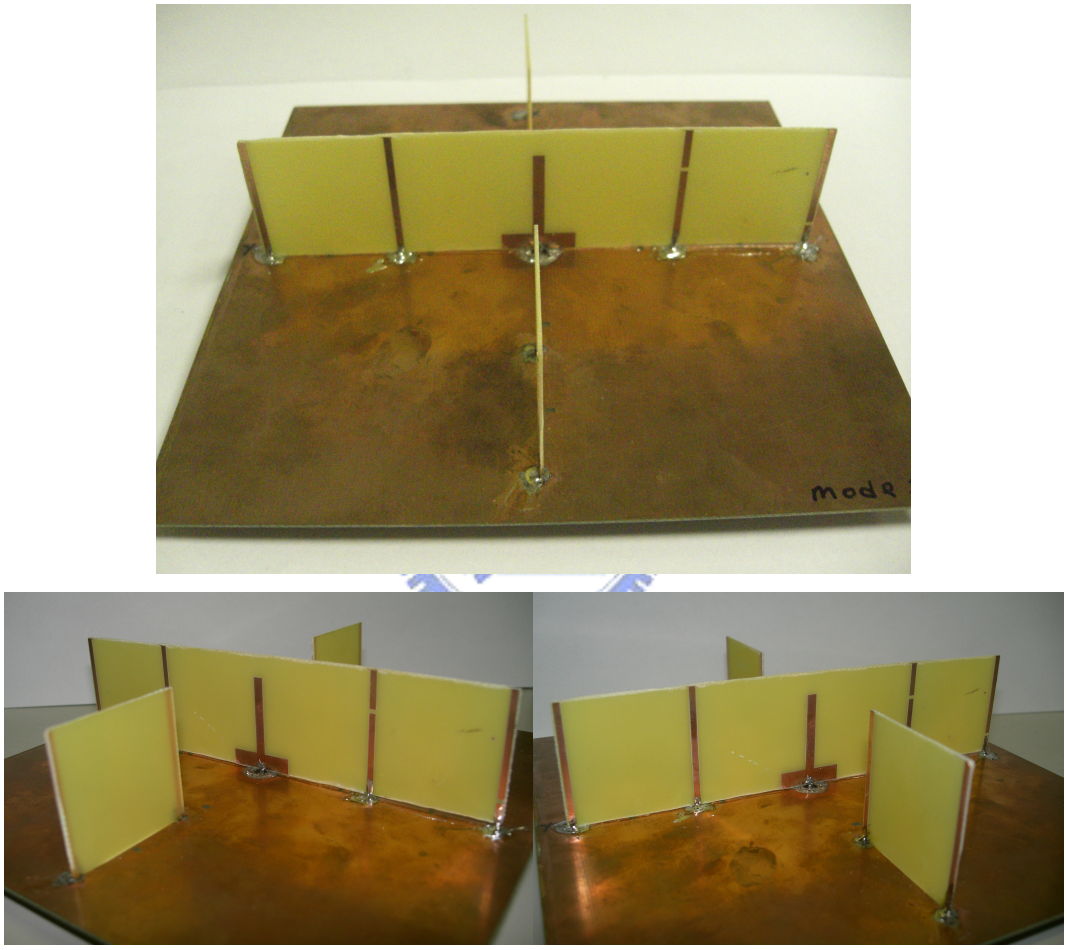

Fig. 4.3.1 Pictures of nine-element array.

4.3.1 Case 1 of nine-element array

Fig. 4.3.1.1 is the measured and simulated return losses of case 1 of nine-element array which is the prototype of the nine-element array in case 1. Due to the added

parasitic elements (A3, A4, B3, and B4), the resonance frequency has shifted to 2.29GHz. The measured bandwidth for reflection coefficient below -10dB is from 2.12 to 2.52 GHz, which includes required bandwidth sufficiently. The pattern of case 1 is displayed in Fig. 4.3.1.2 The SLL on the ϕ = 315° plane is 11.53 dB which has been decreased from simulated one more than 3dB. The F/B (front to back, unit: mm) ratio and HPBW on the ϕ = 315° plane are 32.67 dB and 60°. Comparing with simulated peak gain, the measured peak gain occurred at θ = 50°, ϕ = 315° is increased obviously with value of 7.59dBi. Although the added parasitic elements with switches A3, A4, B3, and B4 improve the peak gain only by 0.64dB, the multiple directivities provided is very attractive.

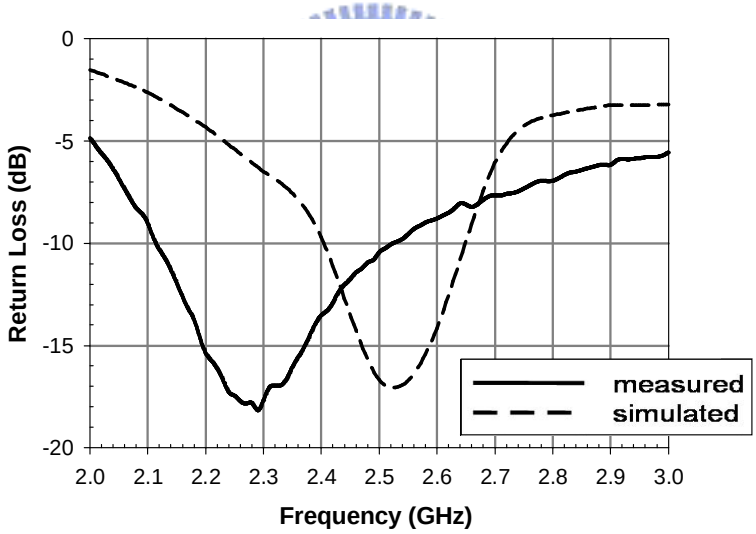

Fig. 4.3.1.1. The measured return loss of case 1.

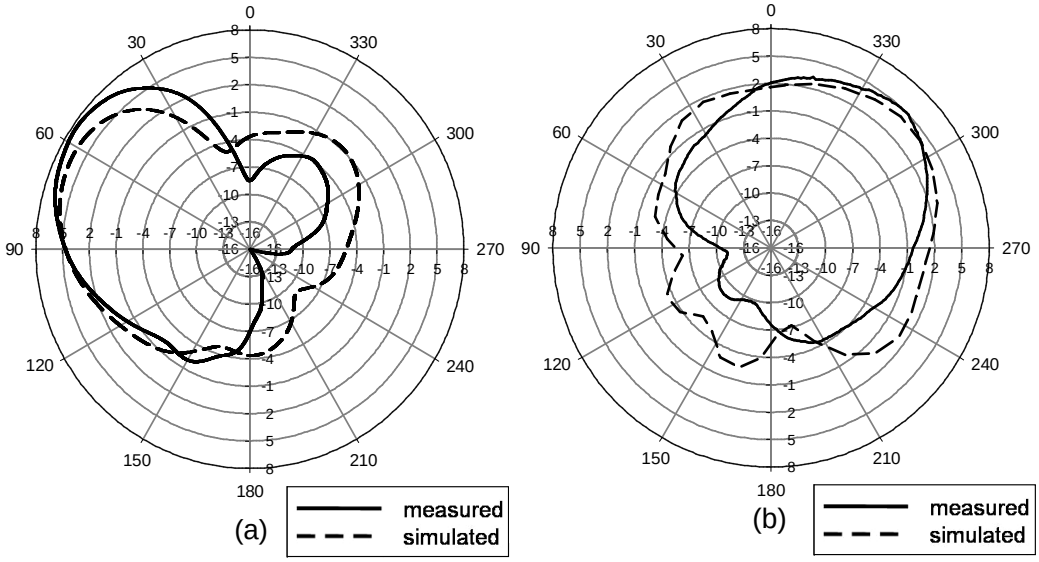

Fig. 4.3.1.2. The measured patterns of case 1 at its center frequency, 2.29GHz. (a) ϕ = 315°plane (b) xy plane

4.3.2 Case 2 of nine-element array

Fig. 4.3.2.1 is the measured and simulated return losses of case 2 of nine-element array which is the prototype of the nine-element array in case 1. The measured bandwidth for reflection coefficient below -10dB is from 2.14 to 2.50 GHz, which includes required bandwidth sufficiently. Although there is still frequency shift from simulated return loss, the bandwidth of case 2 is almost equal to case 1, which is a good property in real application. The pattern of case2 is displayed in Fig. 4.3.2.2. The directivity is similar to simulated one, which has a peak gain on the –y direction and comparatively small side lobes on the y direction. The obvious difference in Fig. 4.3.2.2 xz plane is due to the scale setting in this thesis and the measured pattern on xy plane along x axis. As a result, a switchable main beam direction is provided and the separate angle is 45 degrees in required band by using case 1 and case 2.

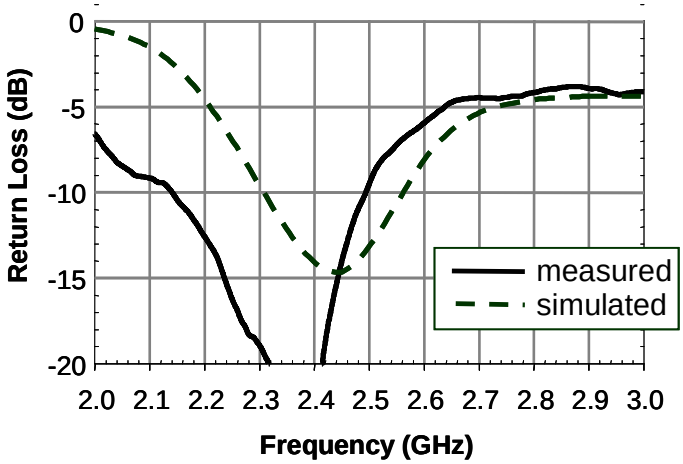

Fig. 4.3.2.1. The measured return loss of case 2.

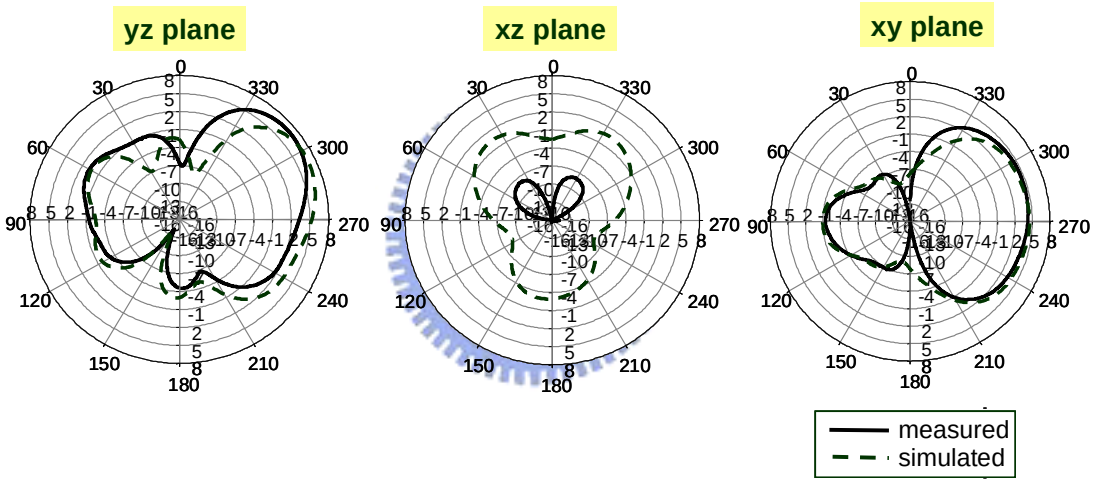

Fig. 4.3.2.2. The measured patterns of case 2.

4.3.3 Case 3 and case 4 of nine-element array

Since case 1 and case 2 provide eight main beam directions covering the whole H plane and include required 2.45GHz band, the proposed antenna configuration is adequate for application in real. In the next, patterns of case 3 and case 4 are disclosed in Fig. 4.3.3.1 and Fig. 4.3.3.2, respectively. From Fig. 4.3.3.1, it is obvious that measured and simulated patterns on yz plane have similar peak gain. But measured

pattern has less side lobe. On xy plane, the measured pattern is pulled by three directors. However, the pull effects of directors are a little different from simulated ones. Fig. 4.3.3.2 shows the measured pattern is alike simulated pattern which has property of bidireciton.

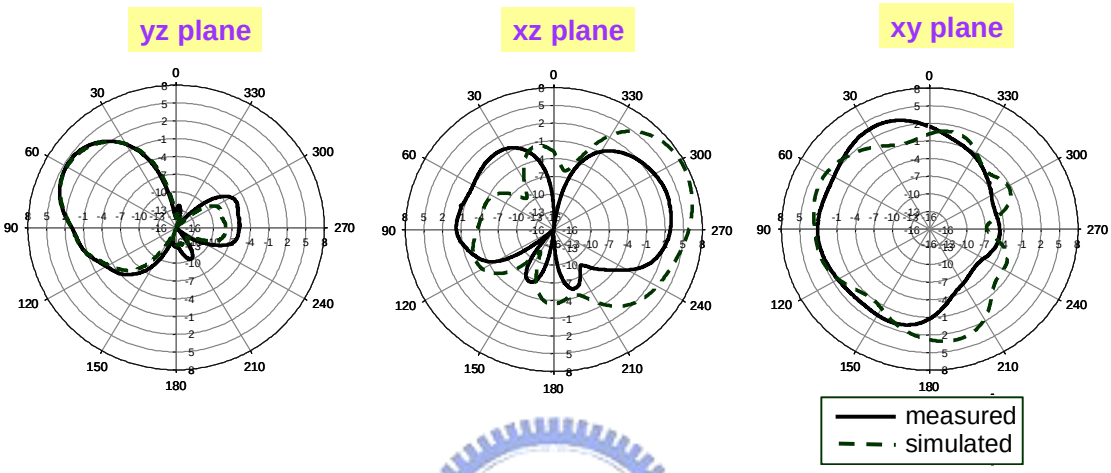

Fig. 4.3.3.1. The measured patterns of case 3.

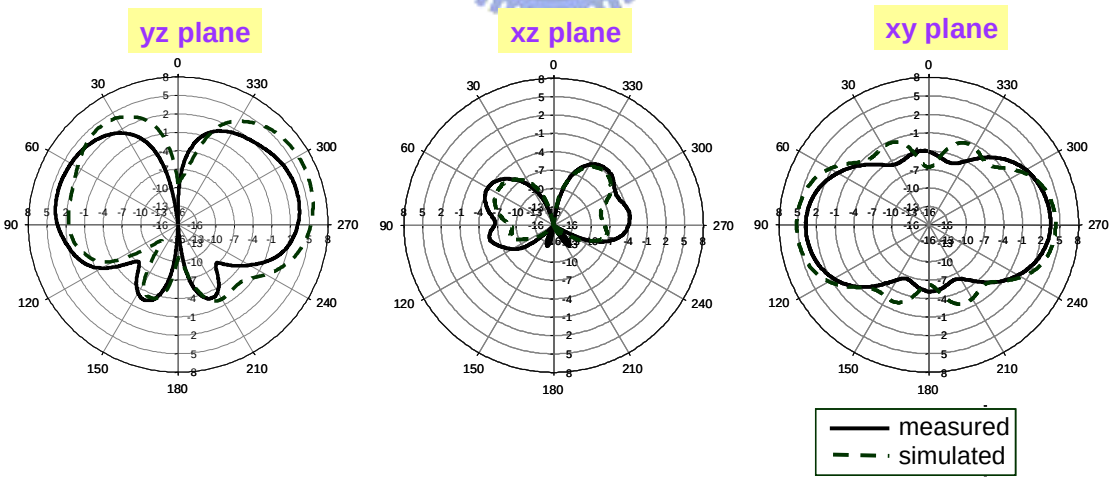

Fig. 4.3.3.2. The measured patterns of case 4.

4.4 Switch effects on radiation pattern

Ideal copper strip and short slot are taken to replace switch on and off. When utilizing pin diode as switch, there are some problems to solve. First, the biasing line layout must not induce unwanted coupling. Second, the pin diode loss must be small with high isolation. Third, the parasitic R, L, and C effects in pin diode must not influence anything of antenna. Unfortunately, because the switch location is on the parasitic element directly, these three problems are unavoidable while enforcing. A simple prototype is established as a reference. A pin diode HMSP 3314 is used as a switch, and set on the position, that is, A1-A4 and B1-B4. Positive bias voltage is supplied by 1.5V battery. A RF choke inductance (15nH) and a DC block capacitor (10pF) are parallel and serial to the switch respectively. RF signal and DC signal share the same ground on xy plane. The extra coupling from the bias line, parasitic RLC of pin are the reason of frequency shift and deformed radiation pattern. Fig.4.4.1 displays the measured (prototype with ideal switch), simulated, and measured (prototype with pin diode switch) radiation pattern of case 1 of nine-element array. The directivity is distorted seriously so the peak gain even decreased 3dB.

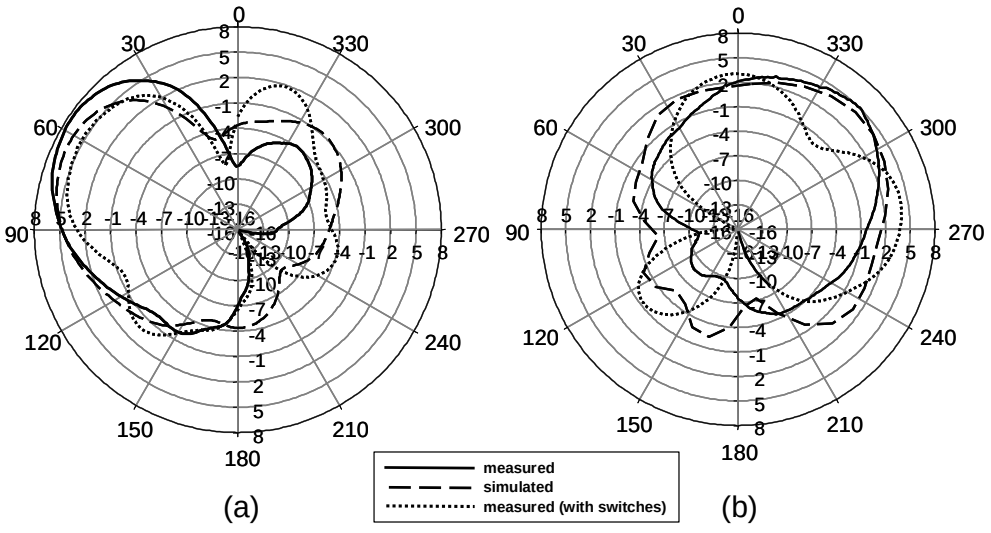

Fig. 4.4.1. The switch effects on radiation pattern.

Chapter 5 Conclusion

A novel kind of radiation pattern reconfigurable antenna configurations is presented. It is not to change the parasitic impedance alternatively by open or short terminations but to maintain the short ended parasitic monopoles modified by switches changing the effective length directly. Printed strip on the FR4 substrate are used as parasitic monopole elements for convenience fabrication instead of conventional three dimensional monopoles. Typical three elements array is shown as a basic reference, and five elements array and nine crisscross elements array are also presented in this paper. Experimental results confirm that the configuration provides high gain with decreasing number of parasitic elements. Three and five elements arrays provide directivity which can be switched 180 degrees by inversely setting switches states. By the method of controlling the switches states, there are four cases with different directivity in the nine elements array, that is, the pattern of nine elements array can be rotated 45 degrees to cover the whole H plane. Among the three, five, and nine elements array, the nine elements array provides multiple directivities and maximum peak gain of 7.59dBi.

References

[1] A. Mehta and D. M. Syahkal, “Spiral antenna with adaptive radiation pattern under electronic control,” *in IEEE AP-S Int. Symp.*, pp. 843-846, June 2004.

[2] A. Mehta, H. Nakano and D. M. Syahkal, “A switched beam single arm rectangular spiral antenna with hybrid switch network,” *in IEEE AP-S Int. Symp.*, pp. 589-592, July 2005.

[3] S. S. L. Yang and L. M. Luk, “A wideband L-probe fed patch antenna for pattern reconfigurable,” *in IEEE AP-S Int. Symp.*, vol. 2B, pp. 581-584, July 2005.

[4] M. D. Migliore, D. Pinchera, and F. Schettino, “A simple and robust adaptive parasitic antenna,” *IEEE Trans. Antennas Propag.*, vol. 53, no. 10, pp. 3262-3272, Oct. 2005.

[5] Y. Nakane, T. Noguchi, and Y. Kuwahara, “Trial casel of adaptive antenna equipped with switched loads on parasitic elements,” *IEEE Trans. Antennas Propag.*, vol. 53, no. 10, pp. 3398-3402, Oct. 2005.

[6] M. R. Kamarudin and P. S. Hall, “ Disc-loaded monopole antenna array for switched beam control,” *IEE Electronics Letters*, vol. 42, Issue 2, pp. 66-67, Jan. 2006.

[7] R. Vaughan, “Switched Parasitic Elements for Antenna Diversity,” *IEEE Trans. Antennas Propag.*, vol. 47, Issue 2, pp. 399-405, Feb. 1999.

[8] H. S. M. Elkamchouchi and H. E. -D. M. Hafez, “Switchable Beam Diversity Antenna,” *in Pro. 2002 3rd Int. Conf. Microwave and Millimeter Wave Technology*, pp. 377 - 380, Aug. 17-19, 2002.

[9] C. Laohapensaeng, C. Free, and K. M. Lum, “Printed strip monopole antenna with the parasitic elements on the circular ground plane,” *in IEEE Int. Workshop in*

Antenna Technology: Small Antennas and Novel Metamaterials, pp. 371-374, March 7-9, 2005.

[10] S. Zhang, G. H. Huff, J. Feng, and J. T. Bernhard, "A pattern reconfigurable microstrip parasitic array," *IEEE Trans. Antennas Propag.*, vol. 52, Issue 10, pp. 2773-2776, Oct. 2004.

[11] G. H. Huff and J. T. Bernhard, "Integration of packaged RF MEMS switches with radiation pattern reconfigurable square spiral microstrip antennas," *IEEE Trans. Antennas Propag.*, vol. 54, Issue 2, Part 1, pp. 464 – 469, Feb. 2006.

[12] C. J. Panagamuwa, A. Chauraya, and J. C. Vardaxoglou, "Frequency and beam reconfigurable antenna using photoconducting switches," *IEEE Trans. Antennas Propag.* ,vol. 54, Issue 2, Part 1, pp. 449-454, Feb. 2006.

[13] N. Behdad, and K. Sarabandi, "Dual-band reconfigurable antenna with a very wide tunability range," *IEEE Trans. Antennas Propag.*, vol. 54, Issue 2, Part 1, pp. 409-416, Feb. 2006.

[14] D. V. Thiel, "Switched parasitic antennas and controlled reactance parasitic antennas: a systems comparison", *in IEEE AP-S Int. Symp.*, , vol. 3, pp. 3211-3214, June 2004.

[15] W. L. Stutzman, G. A. Thiele, *Antenna Theory And Design.* New York: Wiley, 1998

[16] HFSS, Ansoft Corporation, Pittsburgh, PA.